Enhanced Reactivity toward Oxidation by Water Vapor: Interactions of Toluene and NO_2 on Hydrated Magnetite Nanoparticles

Nermin Eltouny and Parisa A. Ariya

Abstract

In the atmosphere, water vapor affects the interaction of trace gases and particles, influencing key processes including cloud nucleation, radiation, and heterogeneous chemistry. In this study, the effect of water vapor on the reactions of toluene and NO_2 on magnetite, a component of atmospheric dust particles, is investigated using a suite of analytical techniques, namely, X-ray photoelectron spectroscopy (XPS) and time-of-flight secondary ion mass spectrometry (TOF SIMS). Adsorption isotherms show that water vapor reduces the adsorption of toluene on magnetite. XPS spectra reveal that exposure to water vapor results in limited dissociation and molecular adsorption of water, and partial oxidation of magnetite. When toluene is added, enhanced dissociation of water and oxidation of the magnetite surface are observed, strongly suggesting the importance of intermolecular interactions between water molecules and the interaction of toluene with the H-bonded network of adsorbed water. Upon addition of NO_2, enhanced oxidation and NO_3 are observed in XPS and TOF SIMS spectra, respectively. In contrast, on oxidized magnetite, less dissociation and sorption of water is observed, and no enhanced oxidation is observed. Our results show that hydrated magnetite surfaces inactive toward further water dissociation can be reactivated depending on the surface chemistry, due to Fe^{2+}. We show that the effect of water vapor on the interaction of toluene and NO_2 on magnetite depends on the Fe^{2+}/Fe^{3+} ratio, which can vary under environmental conditions. Different reactivity of the Fe_3O_4 in dust can thus be expected, with implications on the fate of pollutants in the atmosphere.

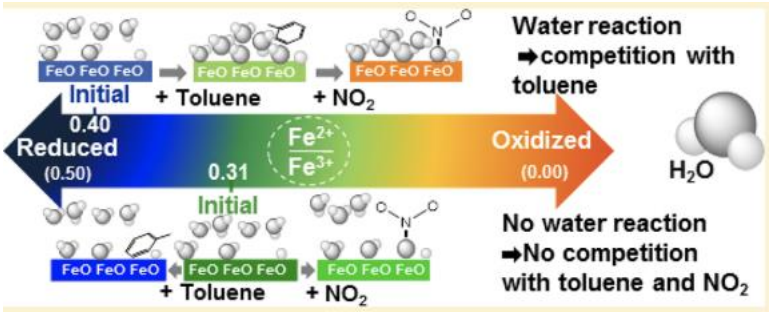

Introduction

Aerosol particles are ubiquitous in the atmosphere. Emitted directly from natural and anthropogenic sources and/or formed from secondary reactions, they interact with radiation and can undergo further reactions with atmospheric constituents that affect air quality and climate.(1) The effect of particles in the atmosphere depends on their physical (e.g., size and shape) and chemical properties. The International Panel on Climate Change (IPCC) fifth Assessment Report (2013) states that despite progress made in understanding the physical and chemical properties and reactions of particles, aerosols and their interactions with clouds and radiation "contribute the largest uncertainty to the total radiative forcing estimate" affecting climate change. The aerosol-cloud-induced uncertainty is as large as the effect of increasing atmospheric concentration of well-mixed greenhouse gases. Current research efforts are dedicated to understanding reactions of particles with gaseous atmospheric constituents, namely, trace gases like water vapor,(2) NO_2,(3) SO_2,(4) and volatile and semivolatile organic compounds.(5)

Iron oxides are an important class of aerosols emitted in the atmosphere from natural and anthropogenic sources.(6) Magnetite ($FeO{\cdot}Fe_2O_3$) is a mixed-valence iron oxide containing $Fe^{2+}$and Fe^{3+} that occurs naturally in rocks and sediments,(6) but is introduced into the atmosphere from anthropogenic activities involving fuel combustion, in particular, from vehicle emissions(7) and in the production of steel.(6) Owing to its diverse properties, sorptive and catalytic in particular, magnetite is of interest to many fields. For instance, in industry, magnetite catalyzes the production of H_2 in the water gas shift reaction(8) and the production of ammonia.(6) For

pollution remediation technology, magnetite is used to remove heavy metals and organic compounds from water(9, 10) and air.(11) In the environment, a recent field study suggested the presence of magnetite in dust could be responsible for the adsorption of polyaromatic hydrocarbons.(12) The sorption capabilities of magnetite demonstrate its significance as an environmental surface.

The interaction of water on solid surfaces has been the subject of considerable research due to its relevance to various fields such as semiconductors,(13) catalysis,(14) and corrosion of metals.(15, 16) In the context of atmospheric chemistry, the adsorption of water or OH/H_2O on the surface of particles will likely influence subsequent interactions with trace gases such as NO_2, SO_2, and organic compounds. Studies on the adsorption of SO_2 on mineral dust components show that the presence of water vapor enhanced the formation of SO_3^{2-} on calcium carbonate(17) but not on α-Fe_2O_3.(18) On aluminum oxide, the coordinated structure of nitrate ion solvated by coadsorbed water was shown to be different from that of the free nitrate ion(19) (and references therein). On magnetite, water is reported to dissociate into OH and H on oxygen vacancies and iron sites at low water concentration, but adsorb molecularly at increasing pressures through hydrogen bonding with surface hydroxyl groups.(20) Therefore, surface properties and different water vapor concentrations (resulting in different coverage) will likely lead to various surface chemistries and reactivity. In addition to water, the presence of multiple gases on certain metal oxide surfaces results in different reactivity. For example, it was reported that the presence of NO_2 and SO_2 could enhance the formation of SO_4 on ZnO, TiO_2, α-Al_2O_3, MgO, and α-Fe_2O_3.(4) Therefore, to evaluate the potential impact of magnetite as an environmental surface on climate and air quality, the effects of water and the coadsorption of multiple trace gases on its surfaces need investigation.

In previous studies,(21, 22) we have shown that aromatics, namely BTEX, adsorbed efficiently to magnetite nanoparticles and that NO_2 competed with toluene at concentrations relevant to polluted areas by oxidizing the surface and forming NO_3 in dry air. However, the impact of coadsorbed water on the reactions of NO_2 and toluene on magnetite was unknown and is the subject of the present work. In this study, we aimed our focus on toluene as a model for BTEX with a vapor pressure between those of the most volatile benzene and the less-volatile ethylbenzene and xylenes. Toluene is more reactive by virtue of its methyl group compared with benzene and is a better model for less-volatile compounds belonging to the BTEX series. The adsorption of toluene in the presence and absence of NO_2 at relative humidity of 50 and 90% was herein investigated by collecting adsorption isotherms using gas chromatography–flame ionization detection (GC-FID). Changes in the chemical composition, which include the Fe^{2+}/Fe^{3+} oxidation ratio and the formation of products were analyzed using XPS and TOF SIMS. Understanding the reactions of toluene, NO_2, and water vapor on magnetite is necessary to predict the impact of rising dust and trace gas emissions on air, water, and soil surrounding urban and industrial areas, as well as on direct air pollution treatment efforts. We discuss the implications of our results in understanding air quality and climate processes.

Experimental Section

Adsorbents Synthesis

The Fe_3O_4 nanoparticles (NPs) were synthesized by coprecipitating a 2:1 solution of $FeCl_3 \cdot 6H_2O$ and $FeCl_2 \cdot 4H_2O$ with ammonium hydroxide in deoxygenated water at 358 K based on the Massart method(23) and modified by Vereda et al.(24) The nanoparticles were dried in a vacuum oven at 323 K and then stored in a vacuum desiccator until needed. The number of washings with water controlled the initial oxidation ratio of the NPs; the higher the number of washings, the more oxidized the Fe_3O_4 NPs.

The NPs were crushed to a powder using a mortar and pestle. For the adsorption isotherm reactions, after weighing, a magnetic stirring bar was used to collect the powder after weighing, a magnetic stirring bar was used to collect the powder; both the powder and the magnet were transferred to the flask, which was then sealed. For the XPS and TOF SIMS reactions, the NPs were weighed on weighing paper and transferred directly to the flasks. A magnet was placed outside the walls of the flask to keep the powder together. For the XPS and TOF SIMS analyses the NPs were transferred onto another weighing paper and then pressed onto the respective tapes used for the analyses. Before and after the addition of NPs, the flask containing a Teflon-coated magnetic stirring bar was evacuated down to at least 2×10^{-2} Torr using a Schlenk vacuum system and kept under vacuum for at least 20 min. The flasks were then filled with ultrahigh purity N_2 and re-evacuated down to a low of 10^{-2}–10^{-3} Torr. This cycle was repeated once more, and after the second evacuation the flask was filled with extra dry air. At this point the selected gases were added.

Adsorbent Characterization

We used several complementary analytical techniques to characterize the Fe_3O_4 NPs. X-ray diffraction (XRD) patterns were recorded on a Siemens D5000 diffractometer with Cu Kα radiation (λ = 1.5418 Å) to identify their crystal structures and average size. Transmission electron microscopy images were taken on a Philips CM200 TEM to investigate the morphology of the Fe_3O_4 NPs. The Brunauer–Emmett–Teller (BET) specific surface area and the Barrett–Joyner–Halenda (BJH) average pore size were determined using a TriStar 3000 V6. 07 A (serial number 2134) surface area analyzer at 77 K. For the surface chemical composition investigation of Fe_3O_4 NPs, we used X-ray photoelectron spectroscopy (ESCALAB 3 MKII de VG) using a nonmonochromatic Al Kα source to collect high-resolution scans of the carbon C 1s, oxygen O 1s, and iron Fe 2p core lines. The charge shift correction was done relative to the adventitious C 1s at 285.0 eV (shown in the Supporting Information). All reported binding energies in this work have a resolution of ±0.4 eV. To analyze potential reaction products sorbed on the surface, time-of-flight secondary ion mass spectrometry (ION-TOF SIMS IV) was performed on the magnetite exposed to various experimental conditions. The Fe_3O_4 NP samples were bombarded with a Bi^+ ion source at 25 kV. Mass to charge spectra for positive and negative ions were collected. Details on the determination of size from XRD and the fitting of XPS spectra are given in the Supporting Information section.

Stock and Reaction Gas Mixtures

Separate and diluted stock mixtures of toluene and NO_2 were freshly prepared and left to equilibrate for 3 h before they were used in experiments. Water vapor was transferred from a flask containing liquid water in equilibrium with its vapor at room temperature (T = 296 ± 1 K). The preparation of reaction mixtures involved transferring water vapor to the required pressure and filling to 1 atm with dry air using a vacuum line, while toluene and NO_2 were transferred using gastight syringes (Hamilton Company USA). Glass flasks were used and were precoated with a hydrophobic layer of GLASSCLAD 18 (UCT Specialties, Inc.). For XPS and TOF SIMS experiments, the reaction mixtures were left for 24 h prior to analyses. Additional details on the preparation of stock mixtures are given in the Supporting Information.

Adsorption Isotherm

Adsorption isotherms of toluene on Fe_3O_4 NPs were measured by the incremental injection of toluene into reference and treatment flasks, which contained water vapor amounting to 50% or 90% relative humidity (RH) in air. The reference flasks contained toluene only and were used to construct a calibration curve. The treatment flasks contained 0.14 g (RH 50%) and 1 g (RH 90%) of magnetite, and toluene alone, or in the presence of 1.5 ppm by volume (ppmv) NO_2. Adsorption isotherms were determined by quantifying the gas-phase concentration of toluene using a preconcentrating CARBOXEN/polydimethylsiloxane (CAR/PDMS) solid-phase microextraction (SPME) fiber coupled with a gas chromatograph equipped with a flame ionization detector (GC-FID-HP 6890). The amount of toluene adsorbed was calculated by subtracting the number of moles at equilibrium in the reaction flask from the initial number of moles, which were determined from the linear fit of the calibration curve, obtained using the reference flask. The amount of toluene adsorbed per gram of Fe_3O_4 NPs as a function of toluene remaining in the gas phase was plotted. Details on chromatography are given in the Supporting Information.

Surface Chemical Analysis

XPS high-resolution spectra for Fe 2p, O 1s, and C 1s were collected for two sets of experiments carried out on two magnetite surfaces of different oxidation ratios, namely, sample series A (Fe^{2+}/Fe^{3+} = 0.46[22]) and sample series B (Fe^{2+}/Fe^{3+} = 0.38[22]). For simplicity, samples from series A or series B are referred to sample A, or B, respectively. For both sets, 0.02 g of magnetite NPs were exposed to an RH of 90% in dry air at 1 atm and room temperature (T =

296 ± 1 K). For sample A, the treatment flasks contained 13 ppmv of toluene in one flask, and a mixture of 0.65 ppmv of NO_2 and 13 ppmv of toluene in another flask. For sample B, an additional flask containing 0.65 ppmv NO_2 only was tested. XPS spectra for dry samples of A and B were also collected.(22) The Fe^{2+}/Fe^{3+} ratio of the surface was calculated from the contributions of Fe^{2+} and Fe^{3+} determined from the fitted peaks in the Fe 2p spectra. The base pressure in the XPS chamber was kept under 10^{-8} Torr. Details on the determination of Fe^{2+}/Fe^{3+} are given in the Supporting Information. For the TOF SIMS analysis, the same preparation procedure as the XPS was followed. For the TOF SIMS, the analysis was carried out on Sample B. For the reactions involving 0.65 ppmv NO_2, the concentrations were too low to be detected by either XPS or TOF SIMS. Therefore, we report the results of an experiment carried out for a sample exposed to 100 ppmv of NO_2 using TOF SIMS.

Materials and Supplies

$FeCl_3 \cdot 6H_2O$ (>98%, Sigma-Aldrich) and $FeCl_2 \cdot 4H_2O$ (≥99%, Sigma-Aldrich), toluene (99.8%, Fisher Scientific), and $NH_3 \cdot H_2O$ (≥25% ammonia, Fisher Scientific) were used as received. NO_2 (1.02% in N_2, Praxair), ultrahigh purity nitrogen (99.999%, MEGS Specialty Gases), and extradry compressed air (content of O_2 19.5%–23.5% and H_2O < 10 ppm, Praxair Canada, Inc.) were used as received. The SPME fibers were purchased from Sigma-Aldrich and conditioned as suggested by the manufacturer. Distilled and deionized water (18.2 MΩ·cm) was obtained from a Milli-Q machine (Simplicity 185). The pressure readings were measured using a capacitance manometer (Model 600 Barocel, Edwards).
Additional information on methodology, and error analysis, are provided in the Supporting Information section.

Results and Discussion

Characterization of Magnetite Nanoparticles

X-ray diffraction patterns were collected to identify the crystal and to determine the size of the nanoparticles. Figure 1 shows that sample series A and B match the reference of magnetite and have an average Scherrer size of 9 nm (previously determined(22) and presented as a modified version in Figure 1). The TEM image in Figure 2 shows that the size distribution of the nanoparticles was in the range of 5–10 nm. The BET surface area and average pore size were previously determined(21) to be 80 ± 10 $m^2 \cdot g^{-1}$ and 10 ± 3 nm, respectively.

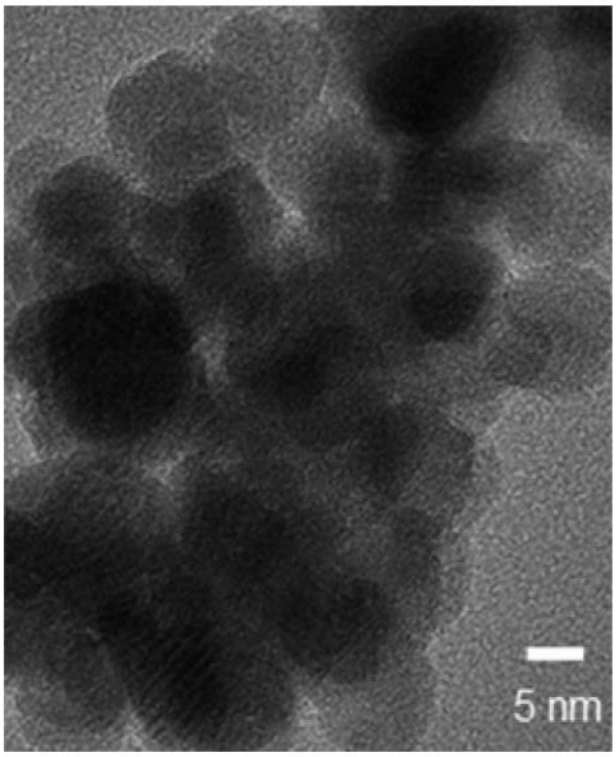

Figure 2. TEM showing the size distribution and crystallinity of magnetite nanoparticles prepared by coprecipitation.

Figure 1. Comparison of XRD patterns of sample series A and B with references for magnetite (JCPDS # 19−069) and maghemite (JCPDS # 39−1346) (Modified from ref 22).

Reduced Adsorption of Toluene Due to Water Vapor

To evaluate the impact of water vapor, we collected adsorption isotherms of toluene at RH of 50% in the presence and absence of NO_2. Figure 3 shows that the adsorption of toluene is inhibited until the equilibrium concentration reaches 0.3×10^{-8} $mol \cdot cm^{-3}$ for RH of 50%. The adsorption of toluene is completely inhibited at RH of 90% (shown in the Supporting Information).

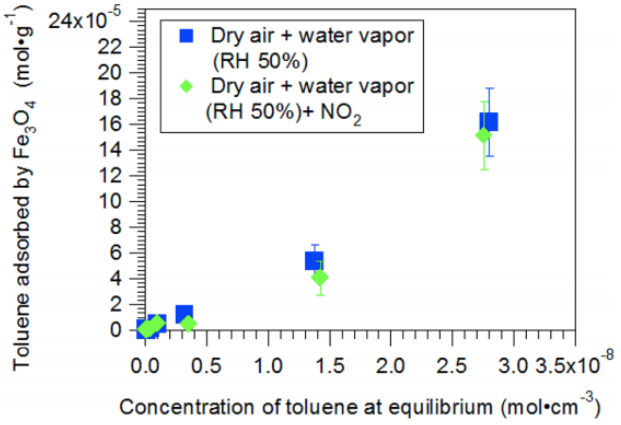

Figure 3. Experimental adsorption isotherms of toluene on magnetite at relative humidity of 50% alone (blue ■) and in the presence of NO_2 (green ◆). Error bars represent standard errors calculated by the propagation of errors during preparation and analyses. Limit of detection is $(2.90 \times 10^{-12}) \pm (1\times 10^{-15})$ mol·cm^{-3}.

In a previous study,(22) the adsorption of toluene on magnetite in dry air resulted in an L-shaped isotherm based on the Giles classification(25) indicating a favorable adsorption. Here, the inverted shape of the isotherm obtained in the presence of water vapor at RH 50% is classified as an S shape. The transition from an L to an S shape is proposed to result from competitive effects, where the competing specie binds strongly to the surface.(25) Therefore, by inspecting the shape of the isotherm, our results suggest that H_2O inhibits the adsorption of toluene by competition for the sites at low toluene concentration. The inflection at higher concentrations of toluene suggests that toluene could be adsorbing by a cooperative mechanism, which has been reported as a possibility for S-shaped isotherms(25) and for the adsorption of toluene on liquid water.(26) With respect to NO_2, the adsorption curves of toluene in Figure 3 coincide. Therefore, on the basis of isotherms alone, the effect of NO_2 cannot be deciphered. To further understand the effect of water vapor and NO_2 (if any) on the adsorption of toluene, we analyzed the surface chemical composition using XPS and TOF SIMS.

Dissociation of Water on Magnetite

To further understand the effect of water vapor and NO_2 on the adsorption of toluene, we analyzed the surface chemical composition using XPS and TOF SIMS. First, we report the effect of water vapor at RH 90% on the oxidation level of the surface of sample series A shown in Figure 4a, which shows that relative humidity causes the oxidation of the surface from Fe^{2+}/Fe^{3+} = 0.46 (previously determined(22)) to 0.40. The analysis of the O 1s spectra in Figure 5a shows five peaks in the O 1s spectrum. The peak at 529.1 ± 0.4 eV is assigned to Fe–O in agreement with reported values.(27) The peak at 530.5 ± 0.4 eV is attributed to Fe–OH and is slightly lower than reported values.(27, 28) The analysis of atomic contributions in the Fe 2p, however, shows that this peak is associated with iron. An additional peak at 526.8 ± 0.4 eV was also added and assigned to an OH at a nonequivalent site.(20) The peaks at 532.2 ± 0.4 eV and 533.9 ± 0.4 eV are assigned to adsorbed OH and H_2O, respectively, and agree with the reported values.(29) Table 1 shows the assignments of the fitted peak and ratios of species calculated from atomic contributions of the O 1s spectrum for sample A. By comparing Fe/O ratios for the dry (previously determined(22)) and humid samples shown in Table 1, a decrease is observed and is consistent with the incorporation of oxygen and the oxidation observed for the Fe^{2+}/Fe^{3+}. The increases in FeOH/FeO from 0.33 (previously determined(22)) to 0.54 indicate that water had dissociated on the iron sites. There is also an increase in peaks higher than 531 eV assigned to OH and H_2O. Note that the binding energies of OH and H_2O also coincide with organic oxygen peaks as shown in

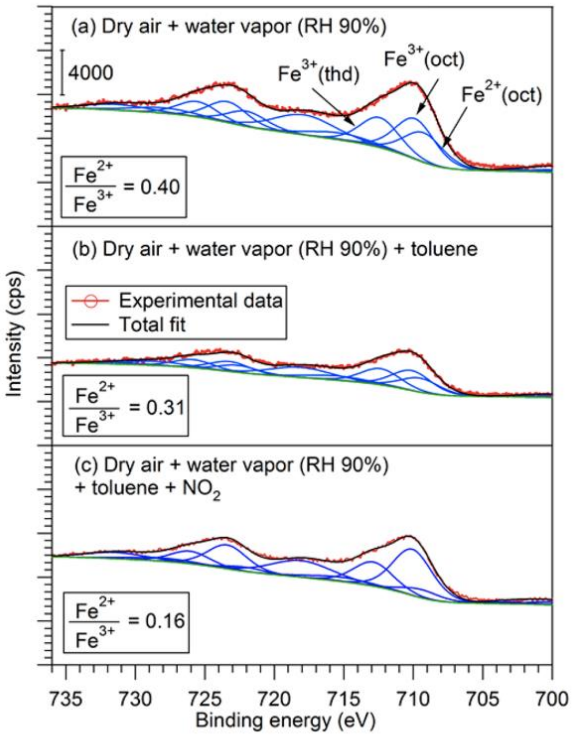

Figure 4. Fe 2p XPS fitted spectra for sample A.

Table 1. By comparing with the C 1s, the peaks at 532.2 ± 0.4 eV and 533.9 ± 0.4 eV are also consistent with organic carbon in the C 1s, which is a common contaminant detected by XPS on samples exposed to air. A recent study on the oxidation of iron by water shows that carbon impurities could dissolve in the water layer giving the C 1s contributions.(30) The formation of OH and adsorption of H_2O are consistent with studies reporting on the partial dissociation of water on magnetite.(20, 31)

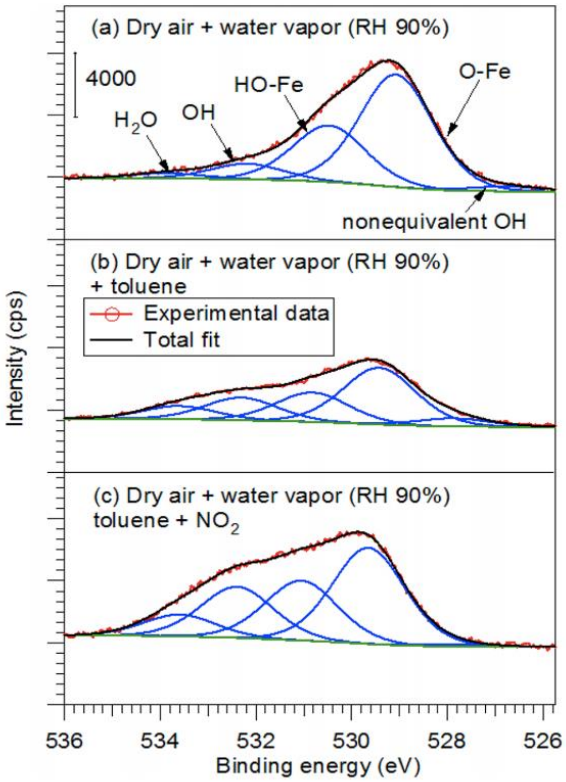

Figure 5. O 1s XPS fitted spectra for sample A.

Table 1. Assignments of O 1s Binding Energies (in eV) and Ratios of Species Calculated from Atomic Percent Contribution of O 1s and Fe 2p XPS High-Resolution Fitted Spectra for Sample A Exposed to Water Vapor (RH 90%)

assigned species: reported literature BE	(a) air	(b) toluene	(c) toluene + NO_2
OH (nonequivalent site) −1.6 (rel. Fe−O), O_2- (undercoordinated) −1 (rel. Fe−O)[20]	526.8	527.9	
O−Fe: 529.9 ± 0.4,[27] 530.1 ± 0.2[28]	529.1	529.4	529.7
HO-Fe: 531.4 ± 0.2,[28] lattice $OH^{\delta-}$: 531.3 ± 0.1[29]	530.5	530.8	531.1
O═C: 531.3, 531.6, 531.9−532.8[55]	532.2	532.3	532.4
adsorbed OH: 532.1 ± 0.1,[29] NO_3 (on TiO_2): 532.5[48]			
O−C: 532.4−533.5,[55] H_2O (adsorbed): 533.3 ± 0.3[29]	533.9	533.6	533.6
Fe^{2+}/Fe^{3+}	$0.40 \pm 2.8 \times 10^{-2}$	$0.31 \pm 3.3 \times 10^{-2}$	$0.16 \pm 1.7 \times 10^{-2}$
Fe/O	$0.70 \pm 2.4 \times 10^{-2}$	$0.54 \pm 2.4 \times 10^{-2}$	$0.47 \pm 1.5 \times 10^{-2}$
O (>531.2 eV)/ O (total)	$0.11 \pm 9.4 \times 10^{-3}$	$0.28 \pm 2.0 \times 10^{-2}$	$0.32 \pm 1.6 \times 10^{-2}$
FeOH (including peak at 528)/FeO	$0.54 \pm 3.3 \times 10^{-2}$	$0.66 \pm 3.8 \times 10^{-2}$	$0.62 \pm 3.9 \times 10^{-2}$

Concerning oxidation, previous studies have reported that exposure to water resulted in the oxidation of iron;(29) here, the presence of Fe^{2+} suggests that the sites for oxidation are not accessible for further dissociation. Studies carried out on similar systems suggest that the inaccessibility to iron cations following exposure to water vapor is due to the presence of H atoms resulting from the dissociation of water, which prevent cation diffusion and occupy sites for dissociation of water.(29) The reduced oxidation of iron could also have occurred due to the presence of water aggregates; recent theoretical studies predict that water aggregates increase the energy barrier for dissociation of water on an iron surface.(32) Other possible explanations for the effect of water on magnetite are described in more detail in the next section.

Increased Dissociation of Water by the Addition of Toluene

To investigate the interaction of toluene on the hydrated surface of magnetite, we analyzed the surface following the addition of toluene at relative humidity of 90% by XPS. In Figure 4b, a decrease in the Fe^{2+}/Fe^{3+} ratio from 0.40 to 0.31 compared with Figure 4a containing water vapor alone is observed.

It is worth noting that we also observe changes in the O 1s spectrum. In Figure 5b, a decrease in the intensity of the O 1s intensity indicates adsorbed species. The ratio of Fe/O decreases, while the contributions at 532.3 eV and at 533.6 eV assigned to OH and H_2O increase. The latter contributions are also consistent with organic carbon in the C 1s. However, because of the possible dissolution of unavoidable contaminants inherent to the technique, it is not possible to determine the identity of the sorbed species causing the reduced intensity of the O 1s and the organic carbon peaks in the C 1s. Nonetheless, upon the addition of toluene, we also observe increases in FeOH/FeO (0.66 in Table 1). An increase in FeOH is consistent with further oxidation of the surface,(33) which could result from further dissociation of water. Furthermore, by comparing with experiments carried out in dry conditions,(22) the FeOH/FeO and O (>531.2 eV)/O (total) ratios are much larger in comparison with the dry sample.(22) These observations suggest that toluene can interact with the hydrated magnetite surface. The increases in the oxidation of the surface and in FeOH and contributions of oxygen at binding energies higher than 531.2 eV point to possible increased adsorption and dissociation of water. At this stage, we cannot confirm the exact mechanism, and in light of the likely contamination appearing in the C 1s and the absence of adsorption of toluene under the same conditions, it cannot be affirmed that toluene is reacting with the adsorbed OH or H_2O. Because the principal sites for water dissociation on Fe_3O_4 are cations,(34) the increase in the OH (532.3 eV) upon the addition of toluene (Figure 5b) indicates iron sites were not saturated with OH or H_2O in Figure 5a; that is, the surface was not completely covered, but those sites were inaccessible for further dissociation. Upon toluene addition, the further increases in OH, water adsorption, and oxidation suggest that toluene can likely interact with the hydrated surface and change the structure of the adsorbed water to favor dissociation. Note that the structural rearrangement and reorientation of dipole of the surface layer of liquid water due to toluene has been proposed.(26) Selected theoretical studies have proposed that the structural arrangement of the water network on metal and their oxides depends on the dissociation site(35, 36) and the coverage.(37) On magnetite nanoparticles having similar sizes as those used here and prepared by coprecipitation, simultaneous growth of water layers at several sites has been reported.(31) Experimental studies on other surfaces report other mechanisms, for example, monomers to three-dimensional icelike structure (on epitaxially grown magnetite),(38) islands (on MgO),(39) and the formation of pseudodissociated water.(40) Some theoretical studies also suggest the rearrangement of hydrogen-bonded OH and H_2O on magnetite (001) is possible.(36) We propose therefore that toluene might likely change the arrangement of the hydrogen-bonded water on the surface into an arrangement that favors dissociation.

A related possibility is that toluene interacts with the network, resulting in the enhanced transfer of proton. Proton transfer via the H-bonded structure of several water molecules has been suggested as the key mechanism that facilitates the dissociation of water at high coverage in comparison with low coverage,(41) which implies the necessity for intermolecular interactions.

The acid–base interaction between water and the benzene ring of aromatics forming icelike cages "trapping" aromatic molecules has been proposed to explain the slight solubility of toluene in water ($T \leq 291$ K).(42, 43) Interactions between the aromatic π and hydrogen on liquid water,(44) from surface OH group on silica(45) (dry and hydrated), and dangling OH on ice(46) have been reported. Though the exact mechanism is unclear, our results strongly suggest the importance of intermolecular interactions between water molecules and the interaction of toluene with the H-bonded network and possible reaction. Future work will include testing the dependence of water dissociation as a function of toluene concentration, as well as the evaluation of the role of molecular O_2, and other key chemical systems of air pollution interest, such as SO_2/toluene/H_2O.

Further Oxidation by NO_2

To investigate whether NO_2 competed with toluene by adsorbing and/or reacting on the hydrated surface of magnetite, we analyzed the surface of magnetite following the addition of NO_2 and toluene at RH of 90% by XPS and by TOF SIMS. A stronger decrease of Fe^{2+}/Fe^{3+} reaching 0.16 is observed, as shown in Figure 4c. Note that

Fe_2O_3 and/or FeOOH are two possible oxidation products(20, 33) in Figure 4, but due to overlaps in binding energies cannot be assigned exclusively. Here again, the addition of NO_2 results in interesting features in the XPS O 1s spectrum in Figure 5c and Table 1. The Fe/O ratio further decreases in comparison with the samples exposed to air and toluene alone indicating further incorporation of oxygen. A slight decrease in the relative contribution of FeOH/FeO for the sample containing toluene alone and an increase in O (>531.2 eV)/O (total) ratio may point to a reaction involving the OH groups. In comparison with the system of toluene (Figure 5b), the overall intensity of the oxygen envelope increases (Figure 5c), indicating there are less adsorbed species. This increase is consistent with an increase in the oxide contribution assigned as FeO and may point to a possible reaction with the adsorbed species when the NO_2 is added. To confirm whether NO_3 was forming on magnetite in the presence of water vapor, TOF SIMS spectra were collected and are shown in Figure 6.

Because this technique is not quantitative, the ion intensities normalized to the total ion intensity were calculated, and as shown in Table 2, samples a–d are comparable; hence, the results obtained under those concentrations are inconclusive. However, the formation of NO_3 is confirmed for a sample exposed to 100 ppmv of NO_2, as shown in Figure 6e. In the presence of H_2O, the formation of NO_3 and the resulting oxidation of magnetite are proposed to occur via reaction 1, which has been reported for HNO_3 formation by heterogeneous hydrolysis of NO_2.(47-49)

$$2NO_2 + H_2O \rightarrow HONO + HNO_3 \quad (1)$$

The formation of HNO_3 via the partial dissociation of NO_2 is proposed to involve a transient species having the form of NO^+NO_3;(49) NO and NO_3 result from the partial dissociation of NO_2 and oxidation of metal oxides.(50) Several species of nitrate on metal oxide in the presence of water have been observed and include HNO_3, solvated and partially solvated nitrate as well as hydronium ion.(51) The dissociation of HNO_3 into NO_3(52) and surface-bound protons was observed on related iron oxyhydroxides.(53) An additional oxidation pathway(54) can also involve the oxidation of the Fe^{2+} following reaction 2:

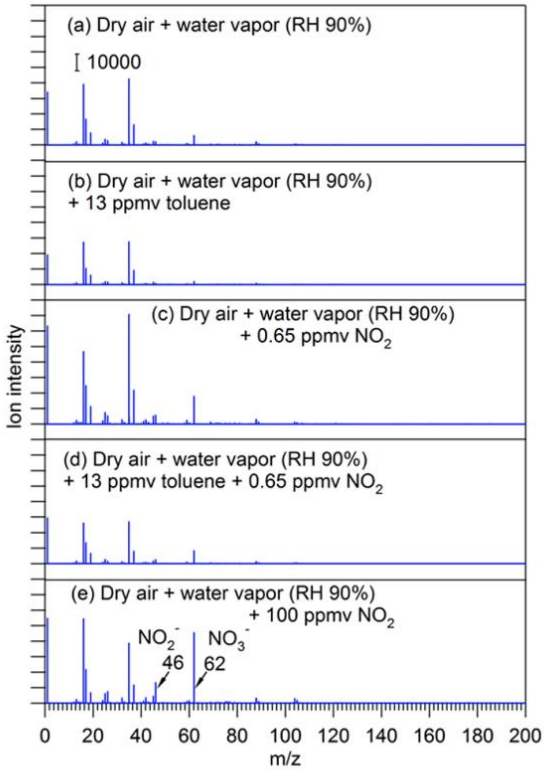

Figure 6. Mass to charge (m/z) spectra obtained by TOF SIMS in negative mode (sample B).

$$3Fe^{2+} + 4H^{+} + NO_3^{-} \leftrightarrow 3Fe^{+} + 2H_2O + NO \quad (2)$$

The increase in Fe–OH observed in Figure 5c could then also result from further dissociation of water on iron sites. Further studies are needed to determine the mechanism(s) resulting in the enhanced oxidation, which could be explained by the dissociation of NO_2, H_2O, and possibly the presence of H^+.

Table 2. Negative Mode TOF SIMS Ion Intensities for NO, NO_2^-, and NO_3^- Normalized by Total Ion Intensity for Samples Exposed to Water Vapor (RH 90%) (sample B)

assignment	NO^-	NO_2^-	NO_3^-
m/z (u)	30.0	46.0	62.0
sample	ion intensities normalized to total ion intensities		
(a) air	$3.72 \times 10^{-4} \pm 1.11 \times 10^{-5}$	$1.22 \times 10^{-2} \pm 6.94 \times 10^{-5}$	$4.02 \times 10^{-2} \pm 1.37 \times 10^{-4}$
(b) 13 ppmv toluene	$3.41 \times 10^{-4} \pm 1.24 \times 10^{-5}$	$7.74 \times 10^{-3} \pm 6.36 \times 10^{-5}$	$2.17 \times 10^{-2} \pm 1.12 \times 10^{-4}$
(c) 0.65 ppmv NO_2	$3.45 \times 10^{-4} \pm 7.87 \times 10^{-6}$	$2.14 \times 10^{-2} \pm 7.06 \times 10^{-5}$	$7.09 \times 10^{-2} \pm 1.43 \times 10^{-4}$
(d) 13 ppmv toluene +0.65 ppmv NO_2	$3.92 \times 10^{-4} \pm 1.31 \times 10^{-5}$	$1.83 \times 10^{-2} \pm 1.00 \times 10^{-4}$	$6.22 \times 10^{-2} \pm 2.04 \times 10^{-4}$
(e) 100 ppmv NO_2	$8.51 \times 10^{-4} \pm 1.28 \times 10^{-5}$	$4.97 \times 10^{-2} \pm 1.19 \times 10^{-4}$	$1.72 \times 10^{-1} \pm 2.58 \times 10^{-4}$

Lower Reactivity on Oxidized Magnetite

To compare the effect of oxidation on the reactivity toward toluene and NO_2 in the presence of water, we carried out the same experiments on a more oxidized sample (sample series B having a ratio of $Fe^{2+}/Fe^{3+} = 0.38$ prior to water vapor exposure).(22) Figure 7a shows that the exposure to water vapor alone results in further oxidation (Fe^{2+}/Fe^{3+} =

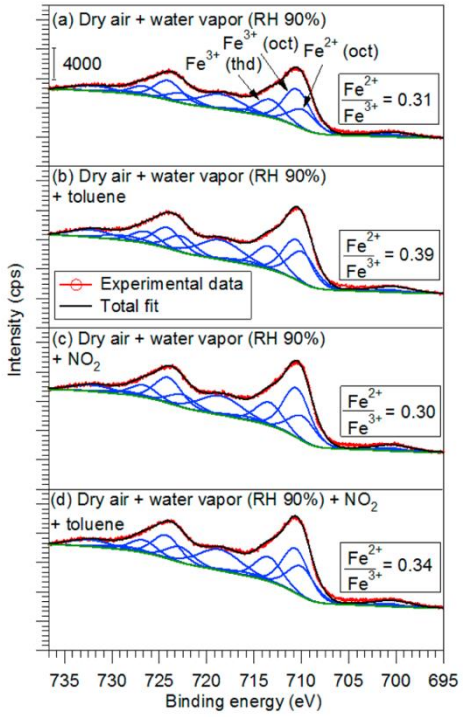

Figure 7. Fe 2p XPS fitted spectra for sample B.

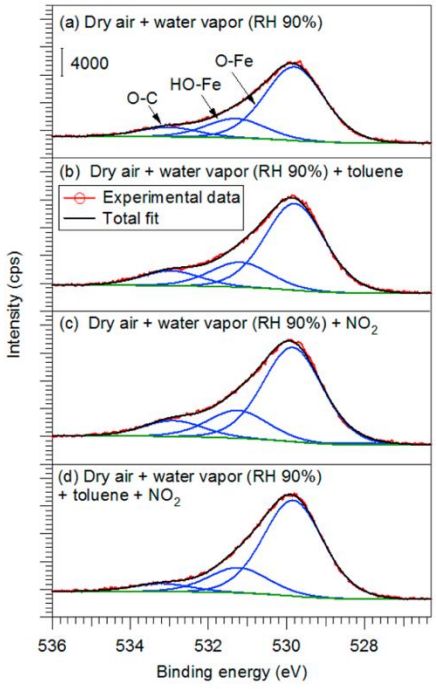

Figure 8. Fe 2p XPS fitted spectra for sample B.

0.31). The O 1s spectrum is shown in Figure 8a, and Table 3 shows the assignments of the fitted peak and ratios based on O 1s and Fe 2p atomic contributions for sample series B. The Fe/O ratio for the sample exposed to water vapor alone is lower than that of the sample in dry air (previously determined(22)), which indicates an incorporation of oxygen and is consistent with the oxidation.

The ratios of FeOH/FeO and organic oxygen increase slightly compared with the dry sample.(22) In addition, contributions assigned to adsorbed OH (532 eV) in sample A are absent in sample B as shown in Figure 8a. These results indicate the oxidized sample is less reactive toward water exposure compared to sample A. The oxygen contribution at 533.0 ± 0.4 eV is also assigned to organic oxygen and consistent with organic carbon in the C 1s. For samples exposed to toluene and the mixture of toluene and NO_2, the Fe^{2+}/Fe^{3+} ratio increases as observed in Figure 7b,d. We have previously observed an increase in the Fe^{2+}/Fe^{3+} ratio in the presence of toluene(21) and a decrease in the presence of NO_2 for experiments carried out in dry air.(22) The Fe/O ratios are also slightly higher for the samples exposed to toluene compared with the blank (no toluene). In Table 4, the TOF SIMS analyses for fractions exposed to toluene show increases in the ion intensities normalized to total ion intensities for fragments associated with toluene at *m*/*z* of 77 ($C_6H_5^+$) and 91 ($C_7H_7^+$), and at *m*/*z* 43 ($C_2H_3O^+$) and 105 ($C_7H_5O^+$), associated with oxygenated compounds, which suggests that toluene is reacting as was previously observed for the reaction of toluene in dry air.(21, 22) The sample exposed to NO_2 alone results in the highest oxidation, which is consistent with the lowest Fe/O (Table 3).

Table 3. Assignments of O 1s Binding Energies (BE) (in eV) and Ratios of Species Calculated from Atomic Percent Contribution of O 1s and Fe 2p XPS High-Resolution Fitted Spectra for Sample B Exposed to Water Vapor (RH 90%)

assigned species: reported literature BE	(a) air	(b) toluene	(c) NO_2	(d) toluene + NO_2
OH (nonequivalent): −1.6, O^{2-} (undercoordinated): −1 (both relative to Fe−O)[20]			527.9	
O−Fe: 529.9 ± 0.4,[27] 530.1 ± 0.2[28]	529.8	529.8	529.8	529.8
HO−Fe: 531.4 ± 0.2,[28] Lattice $OH^{\delta-}$: 531.3 ± 0.1[29]	531.3	531.2	531.2	531.2
O=C: 531.3, 531.6, 531.9−532.8,[55] NO_3: 532.5[48]				
O−C: 532.4−533.5,[55] H_2O adsorbed: 533.3 ± 0.3[29]	533.0	533.0	532.9	533.2
Fe^{2+}/Fe^{3+}	0.31 ± 2.2 × 10^{-2}	0.39 ± 2.4 × 10^{-2}	0.30 ± 1.9 × 10^{-2}	0.34 ± 2.0 × 10^{-2}
Fe/O	0.65 ± 2.1 × 10^{-2}	0.67 ± 2.0 × 10^{-2}	0.62 ± 1.7 × 10^{-2}	0.69 ± 2.0 × 10^{-2}
O (>531.2 eV)/O (total)	0.09 ± 8.0 × 10^{-3}	0.12 ± 8.2 × 10^{-3}	0.11 ± 7.7 × 10^{-3}	0.06 ± 6.0 × 10^{-3}
FeOH (including peak at 528)/FeO	0.26 ± 1.7 × 10^{-2}	0.29 ± 1.7 × 10^{-2}	0.31 ± 1.7 × 10^{-2}	0.26 ± 1.5 × 10^{-2}

Table 4. TOF SIMS of Positive Ion Intensities Normalized to Total Ion Intensities for Oxidized Magnetite (sample B) Exposed to Water Vapor (RH 90%)

assignment	$C_2H_3O^+$	$C_6H_5^+$	$C_7H_7^+$	$C_7H_5O^+$
m/*z* (u)	43.0	77.0	91.1	105.0
sample	ion intensities normalized to total ion intensities			
(a) Air	1.06 × 10^{-2} ± 8.29 × 10^{-5}	2.96 × 10^{-3} ± 4.16 × 10^{-5}	9.72 × 10^{-4} ± 2.33 × 10^{-5}	1.03 × 10^{-3} ± 2.39 × 10^{-5}
(b) 13 ppmv toluene	2.19 × 10^{-2} ± 1.01 × 10^{-4}	4.53 × 10^{-3} ± 4.26 × 10^{-5}	1.54 × 10^{-3} ± 2.41 × 10^{-5}	1.50 × 10^{-3} ± 2.37 × 10^{-5}
(c) 0.65 ppmv NO_2	5.69 × 10^{-3} ± 6.12 × 10^{-5}	1.45 × 10^{-3} ± 2.96 × 10^{-5}	5.66 × 10^{-4} ± 1.82 × 10^{-5}	3.75 × 10^{-4} ± 1.47 × 10^{-5}
(d) 13 ppmv toluene +0.65 ppmv NO_2	2.63 × 10^{-2} ± 1.14 × 10^{-4}	5.79 × 10^{-3} ± 4.94 × 10^{-5}	1.94 × 10^{-3} ± 2.77 × 10^{-5}	2.00 × 10^{-3} ± 2.80 × 10^{-5}
(e) 100 ppmv NO_2	8.15 × 10^{-3} ± 6.44 × 10^{-5}	3.14 × 10^{-3} ± 3.86 × 10^{-5}	9.96 × 10^{-4} ± 2.11 × 10^{-5}	7.35 × 10^{-4} ± 1.80 × 10^{-5}

With respect to oxygen features above 531.3 eV, no significant changes are observed under the various conditions shown in Figure 8; the O/O (total) ratios in Table 3 do not vary by the same extent as sample A (Table 1). These observations suggest that the effect of water is different on oxidized (sample B) and reduced (sample A)

magnetite. Sample B is inactive toward water; that is, the dissociation is not occurring as evidenced by the absence of adsorbed OH (532 eV), and no effect on the subsequent reactions of toluene and NO_2 is observed. In this case, on the oxidized sample, both toluene and NO_2 are able to access the iron sites.

There are several possible explanations for the difference in reactivity toward water between the two samples. The first considers that water dissociation is associated with cations.(34) Compared to magnetite, γ-Fe_2O_3 and FeOOH, which are the probable oxidation phases(29, 33) under our conditions, both have less iron cations in their unit cells.(6) γ-Fe_2O_3 and FeOOH could also passivate the surface toward oxidation due to the presence of Fe^{3+}, which has been suggested to slow diffusion of cations and the rate of oxidation by water vapor.(56) The dissociation of water can also be due to a different termination where surfaces with oxygen are found inactive toward water dissociation for well-defined FeO (111), which is in contrast to well-defined Fe_3O_4 (111) exposing iron cations.(34) The small NPs used here likely have less defined surfaces,(57) and the lower reactivity toward water is attributed to the presence of an oxidized layer for sample B.

Noting that because H_2O is added under vacuum, it is possible that the surface termination of sample A also contained oxygen vacancies, which have been proposed to form on magnetite in oxygen-poor conditions and constitute sites for water dissociation.(36) This is in contrast with oxidized magnetite, which contains an oxidized layer, that is, γ-Fe_2O_3, that contains cation vacancies.(6) The lower reactivity toward water dissociation for sample B suggests that the presence of water does not interact enough with the surface to influence the subsequent interaction of toluene with the magnetite. With respect to NO_2, the detection of NO_3 in Figure 6 can be due to interaction with H_2O as proposed by eq 1 and/or by partial dissociation of NO_2 into NO and NO_3 on the iron resulting in the oxidation observed in Figure 7c; partial dissociation of NO_2 and oxidation of metal centers has been observed on other metal oxides.(50) Though the exact mechanism for the formation of NO_3 cannot be concluded from these results alone, it is apparent that the interaction on sample B is lower compared with sample A, as observed by the extent of oxidation in Figures 7c,d and 4c.

Enhanced Reactivity Due to Fe^{2+}

Because the main difference between samples A and B is the higher stoichiometric Fe^{2+}/Fe^{3+} ratio, the increased reactivity in sample A is attributed to the presence of more Fe^{2+}. The reactivity of Fe^{2+} has been reported in other systems such as aquatic systems where aqueous Fe^{2+} is known to induce the reactivity of other oxide phases with contaminants.(58) For example, increased reactivity toward the reduction of nitrobenzene(59) and uranium(VI)(60) by magnetite have been attributed to the availability of Fe^{2+}. A study by Hoftsetter et al. has shown that both structural and bound Fe^{2+} contribute to reactivity.(61) Furthermore, in light of recent studies reporting on the enhanced oxidation of Fe due to nanoscale size induced forces, which cause faster diffusion of oxygen atoms(62) in addition to the migration of Fe^{2+} to the surface, it is possible that enhanced oxidation of Fe^{2+} is occurring due to nanoscale effects. In our work, though the Fe^{2+} is structural and not in an aqueous form, it is possible that at 90% RH, a combined effect of increased ion diffusion resulting from the size of the nanoparticles (Figures 1 and 2) and the presence of Fe^{2+} explain the reactivity of sample A toward water, toluene, and NO_2. Additional considerations that can affect the reactivity toward toluene and NO_2 include the impact of dissociated products (like OH and H), which in recent theoretical studies point to the significance of charge rearrangement and the dependence on termination to explain catalytic activity of magnetite reactivity.(36) Finally, the phase of oxidized iron (e.g., FeOOH) could also influence the reactivity.

Conclusion

In this work, we investigated the effect of relative humidity on the adsorption and reactions of toluene and NO_2 on magnetite nanoparticles. We showed that water competed with toluene for active sites on magnetite and that the interaction of water on magnetite resulted in OH and molecularly adsorbed water, which are suggested to be the competing species. We found that the initial stoichiometric ratio of magnetite influenced the extent of dissociation of water, in turn influencing subsequent interactions of toluene and NO_2 with magnetite. On reduced samples, higher dissociation of water was observed; the subsequent addition of toluene resulted in additional oxidation, dissociation of water, and possibly the formation of organic species, which suggests toluene interacts with the H-bonded network of adsorbed water. Selected theoretical studies on well-defined surfaces show that various structures of adsorbed

water bonding via a hydrogen network can exist (ice, hydronium) and that adsorbed species can influence the reactivity toward water dissociation;(63) current research also shows the significance of cooperative adsorption of water on dissociation.(20) Our work shows that species like toluene are able to increase water dissociation, possibly by influencing the cooperative adsorption of water on surfaces of environmental relevance. Interestingly, in the case of NO_2, the nearly complete oxidation suggests that the presence of water on the surface results in additional complex pathways. In contrast, on oxidized magnetite samples, water dissociation occurs to a much lower extent and does not influence the interaction of toluene and NO_2. On the basis of the observed changes in oxidation of the surface, the effect of water vapor on the interaction of toluene and NO_2 will vary depending on the stoichiometric ratio of magnetite.

Our results show that hydrated surfaces inactive toward further water dissociation can be reactivated toward more oxidation in the presence of pollutants like toluene and NO_2 depending on the surface chemistry, which includes the availability of Fe^{2+} and adsorbed species. Hence, the potential occurrence of a range of stoichiometric ratios of magnetite in urban dusts will likely affect the fate of pollutants like NO_2 and toluene in humid polluted atmospheres. Therefore, future work should involve testing reactivity at different stoichiometric ratios to establish a clearer relationship between reactivity, stoichiometry, and active sites as well as the identification of products to better evaluate the fate of such reactions on the environment.

Supporting information

Details on the collection and interpretation of XPS spectra, the preparation of stock mixtures, data collection using chromatography, the adsorption isotherm at 90% relative humidity, XPS spectra for C 1s, N 1s, and Cl 2p, and the calculation of XPS and TOF SIMS errors. This material is available free of charge via the Internet at http://pubs.acs.org.

AUTHOR INFORMATION

Corresponding Author
*E-mail: parisa.ariya@mcgill.ca.

Author Contributions
The manuscript was written through contributions of all authors.

Funding
We cordially thank NSERC, FRQNT and Environment Canada for financial support funds.

Notes
The authors declare no competing financial interest.

ACKNOWLEDGMENTS

We are very grateful to Dr. J. Lefebvre for collecting XPS and TOF SIMS spectra and for discussions on XPS and TOF SIMS interpretation. We thank Dr. Y. Nazarenko, Dr. Z. Hu, and Ms. O. Cavaliere for proofreading the manuscript. We acknowledge anonymous reviewers and the editor for providing constructive comments to improve this manuscript.

References

(1) Seinfeld, J. H. P. S. N. *Atmospheric chemistry and physics: from air pollution to climate change;* J. Wiley: Hoboken, N.J., 2006.
(2) Rubasinghege, G.; Grassian, V. H. *Chem. Commun. (Cambridge, U. K.)* 2013, *49*, 3071.
(3) Wu, L. Y.; Tong, S. R.; Ge, M. F. *J. Phys. Chem. A* 2013, *117*, 4937.
(4) Ma, Q.; Liu, Y.; He, H. *J. Phys. Chem. A* 2008, *112*, 6630.
(5) Shen, X.; Zhao, Y.; Chen, Z.; Huang, D. *Atmos. Environ.* 2013, *68*, 297.

(6) Cornell, R. M.; Schwertmann, U. *The iron oxides: structure, properties, reactions, occurrence, and uses*, 2003 ed.; VCH: New York, 1996.
(7) Bucko, M. S.; Mattila, O.-P.; Chrobak, A.; Ziołkowski, G.; Johanson, B.; Čuda, J.; Filip, J.; Zboril, R.; Pesonen, L. J.; Leppäniemi, M. *Geophys. J. Int.* 2013, *195*, 159.
(8) Wang, X. J.; Renn, J.; Spencer, J.; Ratnasamy, C.; Cai, Y. A Novel Method for Measuring Active Sites of Fe_3O_4 for WGS Reaction. *Top. Catal.* [Online early access]. DOI: 10.1007/s11244-013-0126-y. Published Online: 2013.
(9) Mayo, J. T.; Yavuz, C.; Yean, S.; Cong, L.; Shipley, H.; Yu, W.; Falkner, J.; Kan, A.; Tomson, M.; Colvin, V. L. *Sci. Technol. Adv. Mater.* 2007, *8*, 71.
(10) Giraldo, L.; Erto, A.; Moreno-Piraján J. *Adsorption* 2013, *19*, 465.
(11) Dong, J.; Xu, Z.; Kuznicki, S. M. *Environ. Sci. Technol.* 2009, *43*, 3266.
(12) Jordanova, D.; Jordanova, N.; Lanos, P.; Petrov, P.; Tsacheva, T. *Geochem., Geophys., Geosyst.* 2012, *13*, Q08Z49.
(13) Rastgar, N.; Rowe, D. J.; Anthony, R. J.; Merritt, B. A.; Kortshagen, U. R.; Aydil, E. S. *J. Phys. Chem. C* 2013, *117*, 4211.
(14) Hadjiivanov, K.; Knozinger, H.; Tsyntsarski, B.; Dimitrov, L. *Catal. Lett.* 1999, *62*, 35.
(15) Saunders, S. R. J.; Monteiro, M.; Rizzo, F. *Prog. Mater. Sci.* 2008, *53*, 775.
(16) Henderson, M. A. *Surf. Sci. Rep.* 2002, *46*, 1.
(17) Baltrusaitis, J.; Usher, C. R.; Grassian, V. H. *Phys. Chem. Chem. Phys.* 2007, *9*, 3011.
(18) Baltrusaitis, J.; Cwiertny, D. M.; Grassian, V. H. *Phys. Chem. Chem. Phys.* 2007, *9*, 5542.
(19) Grassian, V. H. *Surf. Sci.* 2008, *602*, 2955.
(20) Kendelewicz, T.; Kaya, S.; Newberg, J. T.; Bluhm, H.; Mulakaluri, N.; Moritz, W.; Scheffler, M.; Nilsson, A.; Pentcheva, R.; Brown, G. E. *J. Phys. Chem. C* 2013, *117*, 2719.
(21) Eltouny, N. A.; Ariya, P. A. *Ind. Eng. Chem. Res.* 2012, *51*, 12787.
(22) Eltouny, N.; AriyaP. A. Competing reactions of selected atmospheric gases on Fe_3O_4 nanoparticles surfaces. *Phys. Chem. Chem. Phys.* 2014, DOI: 10.1039/C4CP02379J.
(23) Massart, R. *IEEE Trans. Magn.* 1981, *17*, 1247.
(24) Vereda, F.; de Vicente, J.; Hidalgo-Álvarez, R. *Langmuir* 2007, *23*, 3581.
(25) Giles, C. H.; D'Silva, A. P.; Easton, I. A. *J. Colloid Interface Sci.* 1974, *47*, 766.
(26) Hauxwell, F.; Ottewill, R. H. *J. Colloid Interface Sci.* 1968, *28*, 514.
(27) Poulin, S.; França R.; Moreau-Bélanger, L.; Sacher, E. *J. Phys. Chem. C* 2010, *114*, 10711.
(28) Mills, P.; Sullivan, J. L. *J. Phys. D: Appl. Phys.* 1983, *16*, 723.
(29) Grosvenor, A. P.; Kobe, B. A.; McIntyre, N. S. *Surf. Sci.* 2004, *572*, 217.
(30) Volgmann, K.; Voigts, F.; Maus-Friedrichs, W. *Surf. Sci.* 2012, *606*, 858.
(31) Tombácz, E.; Hajdú, A. l.; Illés, E. b.; László, K.; Garberoglio, G.; Jedlovszky, P. l. *Langmuir* 2009, *25*, 13007.
(32) Freitas, R. R. Q.; Rivelino, R.; de Brito Mota, F.; de Castilho, C. M. C. *J. Phys. Chem. C* 2012, *116*, 20306.
(33) Grosvenor, A. P.; Kobe, B. A.; McIntyre, N. S. *Surf. Interface Anal.* 2004, *36*, 1637.
(34) Joseph, Y.; Ranke, W.; Weiss, W. *J. Phys. Chem. B* 2000, *104*, 3224.
(35) Yu, X.; Li, Y.; Li, Y.-W.; Wang, J.; Jiao, H. *J. Phys. Chem. C* 2013, *117*, 7648.
(36) Mulakaluri, N.; Pentcheva, R.; Wieland, M.; Moritz, W.; Scheffler, M. *Phys. Rev. Lett.* 2009, *103*, 176102.
(37) Grillo, M. E.; Finnis, M. W.; Ranke, W. *Phys. Rev. B: Condens. Matter Mater. Phys.* 2008, *77*, 075407.
(38) Leist, U.; Ranke, W.; Al-Shamery, K. *Phys. Chem. Chem. Phys.* 2003, *5*, 2435.
(39) Foster, M.; D'Agostino, M.; Passno, D. *Surf. Sci.* 2005, *590*, 31.
(40) Cutting, R. S.; Muryn, C. A.; Vaughan, D. J.; Thornton, G. *Surf. Sci.* 2008, *602*, 1155.
(41) Zhou, C.; Zhang, Q.; Chen, L.; Han, B.; Ni, G.; Wu, J.; Garg, D.; Cheng, H. *J. Phys. Chem. C* 2010, *114*, 21405.
(42) Bohon, R. L.; Claussen, W. F. *J. Am. Chem. Soc.* 1951, *73*, 1571.
(43) Shinoda, K. *J. Phys. Chem.* 1977, *81*, 1300.
(44) Gierszal, K. P.; Davis, J. G.; Hands, M. D.; Wilcox, D. S.; Slipchenko, L. V.; Ben-Amotz, D. *J. Phys. Chem. Lett.* 2011, *2*, 2930.
(45) Ringwald, S. C.; Pemberton, J. E. *Environ. Sci. Technol.* 2000, *34*, 259.

(46) Mészár, Z. E.; Hantal, G.; Picaud, S.; Jedlovszky, P. *J. Phys. Chem. C* 2013, *117*, 6719.
(47) Goodman, A. L.; Underwood, G. M.; Grassian, V. H. *J. Phys. Chem. A* 1999, *103*, 7217.
(48) Haubrich, J.; Quiller, R. G.; Benz, L.; Liu, Z.; Friend, C. M. *Langmuir* 2010, *26*, 2445.
(49) Finlayson-Pitts, B. J.; Wingen, L. M.; Sumner, A. L.; Syomin, D.; Ramazan, K. A. *Phys. Chem. Chem. Phys.* 2003, *5*, 223.
(50) Rodriguez, J. A.; Jirsak, T.; Liu, G.; Hrbek, J.; Dvorak, J.; Maiti, A. *J. Am. Chem. Soc.* 2001, *123*, 9597.
(51) Baltrusaitis, J.; Schuttlefield, J.; Jensen, J. H.; Grassian, V. H. *Phys. Chem. Chem. Phys.* 2007, *9*, 4970.
(52) Frinak, E. K.; Wermeille, S. J.; Mashburn, C. D.; Tolbert, M. A.; Pursell, C. J. *J. Phys. Chem. A* 2004, *108*, 1560.
(53) Wijenayaka, L. A.; Rubasinghege, G.; Baltrusaitis, J.; Grassian, V. H. *J. Phys. Chem. C* 2012, *116*, 12566.
(54) Epstein, I. R.; Kustin, K.; Warshaw, L. J. *J. Am. Chem. Soc.* 1980, *102*, 3751.
(55) Beamson, G. B. D. *High resolution XPS of organic polymers: the Scienta ESCA300 database;* Wiley: Chichester, U.K., 1992.
(56) Roosendaal, S. J.; Bakker, J. P. R.; Vredenberg, A. M.; Habraken, F. H. P. M. *Surf. Sci.* 2001, *494*, 197.
(57) Nyiró-Kósa, I.; Nagy, D. C.; Posfai, M. *Eur. J. Mineral.* 2009, *21*, 293.
(58) Williams, A. G. B.; Scherer, M. M. *Environ. Sci. Technol.* 2004, *38*, 4782.
(59) Gorski, C. A.; Scherer, M. M. *Environ. Sci. Technol.* 2009, *43*, 3675.
(60) Latta, D. E.; Gorski, C. A.; Boyanov, M. I.; O'Loughlin, E. J.; Kemner, K. M.; Scherer, M. M. *Environ. Sci. Technol.* 2012, *46*, 778.
(61) Hofstetter, T. B.; Schwarzenbach, R. P.; Haderlein, S. B. *Environ. Sci. Technol.* 2002, *37*, 519.
(62) Pratt, A.; Lari, L.; Hovorka, O.; Shah, A.; Woffinden, C.; Tear, S. P.; Binns, C.; Kröger, R. *Nat. Mater.* 2013, *13*, 26; DOI: 10.1038/ nmat3785.
(63) Mulakaluri, N.; Pentcheva, R.; Scheffler, M. *J. Phys. Chem. C* 2010, *114*, 11148.